

Investigations on physical properties and ablation processes of snow cover during the spring snowmelt period in the headwater region of the Irtysh River, Chinese Altai Mountains

Wei Zhang^{1,2} · Yongping Shen¹ · Ninglian Wang¹ · Jianqiao He¹ · An'an Chen^{1,2} · Jian Zhou¹

Received: 24 December 2014 / Accepted: 7 September 2015 / Published online: 25 January 2016
© Springer-Verlag Berlin Heidelberg 2015

Abstract To explore the effects of the underlying surface on snow properties and the “forest effects” on snow accumulation and ablation processes in the headwater area of the Irtysh River in the Chinese Altai Mountains, the physical properties of snow and certain snowmelt processes were investigated during the snowmelt period in 2014. Our observations showed that the diurnal and daily variations of air and snow temperatures, the liquid water contents (LWCs), and the densities of surface snow layers at 0–5 cm depths were in agreement, but differences in snow properties were obvious at the bottom snow layers. The LWCs were divided into three categories according to snow temperature (T_s): $LWC = 0$, $T_s < -3$ °C; $LWC < 1$ %, $-3 \leq T_s < -1$ °C; $LWC < 7$ %, $T_s \geq -1$ °C. The snow densities were greatest in the top layers above all

underlying surfaces (grassland, concrete, and river ice) during the snowmelt period. The snowmelt experiment indicated that the mean air temperature was the highest on the grassland and lowest in the glade, but the diurnal temperature range was the lowest in the continuous forest and highest on the grassland. The canopy snow interception rate of *Abies sibirica* reached up to 70 % and the mean value of the continuous forest cover was about 30 %. The snowmelt duration periods were 20 days on the grassland, 35 days in the continuous forest, and 43 days in the forest glade, and the corresponding average snow melt rates (SMRs) were 2.1, 1.2, and 1.4 mm d⁻¹. For one single *A. sibirica* tree, the SMR in the sub-canopy was only half that on the edge and outside of the forest canopy.

Keywords Snow cover · Snow physical properties · Snow melt · Forest · Altai Mountains

✉ Wei Zhang
zhangw06@lzb.ac.cn

Yongping Shen
shenyp@lzb.ac.cn

Ninglian Wang
nlwang@lzb.ac.cn

Jianqiao He
hejqcn@lzb.ac.cn

An'an Chen
chenanan1126@163.com

Jian Zhou
zhoujian@lzb.ac.cn

¹ State Key Laboratory of Cryospheric Sciences, Cold and Arid Regions Environmental and Engineering Research Institute, Chinese Academy of Sciences, 320 West Donggang Road, Lanzhou 730000, Gansu, China

² University of Chinese Academy of Sciences, Beijing 100049, China

Introduction

Since the 1980s, in the Northern hemisphere the snow cover distributions from late winter to early summer have declined (Robinson and Frei 2000). In some snow-dominated basins the limited freshwater derived from snowmelt in spring is still vital to human life, agriculture, and industry (Barnett et al. 2005), so in certain arid and semi-arid regions, including northwestern China (Piao et al. 2010), the water resources reserved for ecology have been diverted for irrigation agriculture. This has resulted in fatal damage to local and surrounding natural environments (Wang et al. 2002). The accurate assessment and rational utilization of water resources from spring snowmelt could, to a certain degree, guarantee the regional water supplements and ecological water requirements. However,

climate change and increased human activities have created more uncertainty in the interannual changes of the snow cover, including snow properties, depth, spatial and temporal distributions, and accumulation and ablation processes. Subsequently, those snow changes will affect the atmosphere, hydrosphere, and biosphere by changing the surface energy balance and the water budget.

Snow temperature, liquid water content (LWC), and snow density are the most important variables to describe the basic physical properties of snow cover (Bormann et al. 2013; Burns et al. 2013; Sturm et al. 1997; Takala et al. 2011). Snow temperature is a reliable indicator of snow internal energy, U . Apart from energy exchange with the ground soil and the atmosphere, snow ablation and refreezing processes are mainly controlled by the snow temperature. Temperature gradients of the snow cover notably affect vapor transport, crystal growth and evolution, and deep frost processes. Moreover, the stresses between adjacent snow layers are caused by the differences of snow temperatures and temperature gradients, which are significant inducements to snow avalanche formation and have been widely researched (Schweizer et al. 2003, 2008).

Liquid water in the snowpack, mainly derived from rainfall and snowmelt, has a significant influence on snow physical properties (such as snow density), thermal properties (e.g., thermal content, heat conductivity), and photoelectric properties (such as albedo) (Avanzi et al. 2014; Essery et al. 2013). Variations of LWC will also alter the snow energy and water balances, the stress field of the snow cover, melting and refreezing, and snow redistribution caused by blowing snow (Sundstrom et al. 2013; Techel and Pielmeier 2011). In addition, LWC also affects water and ion transfers in snow cover (Bartels-Rausch et al. 2014) as well as microbe habitat within the snowpack and in the surface soil layer beneath the snow cover.

Snow density is basic data to obtain snow water equivalents, but continuous and accurate long-term observations of snow density are relatively scarce due to limitations of field equipment and technology, except for across the former U.S.S.R. (Zhong et al. 2014). Instead, in some simulation studies the snow density, including the initial value is estimated by parameter optimization algorithms like the Bayesian algorithm (Zhou et al. 2013). The snow density is mostly regarded as an intermediate variable to calculate another relative parameter, such as the heat conductivity of snow cover (Satyawali and Singh 2008; Sturm et al. 1997). With the development of advanced measuring instruments, such as “Finnish Snow Fork”, a radiowave sensor manufactured by the University of Helsinki in Finland, (Techel and Pielmeier 2011), comprehensive and accurate measurements of snow density are now practical, which is conducive to further understanding of the physical properties of snow.

Compared with rainfall runoff, snowmelt runoff processes are more regular because of typical diurnal changes of air temperature and solar radiation, which directly control snowmelt processes. In a snow-dominated basin, snowmelt is usually the main source of spring flood (Jeevani et al. 2012; Khadka et al. 2014). In hydrology, confluence time is an important parameter to forecast flood processes and flood peak evolution formed by snow and glacier melt or extreme precipitation in hydrology. It is also a key parameter that is widely utilized in simulating snowmelt hydrological processes, such as Cold regions hydrological model (CRHM) platform (Pomeroy et al. 2007; Zhou et al. 2014).

In mid- and high-latitude mountainous areas, the distributions of snow cover and forest cover are often highly overlapped (Brown and Robinson 2011; Pan et al. 2013) and the influence of forest cover on snow accumulation and ablation is complex (Varhola et al. 2010). Sublimation losses of snowfall intercepted by the canopy are the main reason why snow accumulation in the sub-canopy is usually less than on non-forest land, but the reduced snow amount widely vary because of the differences of forest coverage, composition, canopy density, forest stand, and tree form (Molotch et al. 2007; Pomeroy et al. 1998, 2002). In addition, decreasing downwelling shortwave radiation and increasing downwelling longwave radiation in the sub-canopy (Essery et al. 2008; Pomeroy et al. 2008) make snow ablation processes in forest areas different from those in open fields. The sensible and latent heat beneath a forest canopy varies widely under the influence of wind (Varhola et al. 2010). Therefore, the snowmelt processes and snowmelt rates (SMRs) are spatiotemporally heterogeneous, which contribute to the difficulty in simulation and prediction of snow hydrological processes.

The Irtysh River originates in the southern slope of the middle Altai Mountains, which form the divide between Mongolia on one side and Russia and China on the other. At 4248 km, it is the longest tributary of the Ob River (Surazakov et al. 2007). Meltwater is the major source of spring surface runoff in the headwater of Irtysh River. In recent years, a lot of artificial building materials, mainly the concrete, was used for engineering constructions in Chinese Altai Mountains, which changed the underlying surfaces to some extent. In addition, the snow cover on the river ice significantly affected the formation and development, and thermal regime of river ice.

On the basis of past field observations taken at the Kuwei snow station constructed in 2011, further detailed experiments were conducted in March and April, 2014. Layered snow temperature, LWC, and snow density on grassland, river ice, and concrete were monitored to estimate the influence of those underlying surfaces on the snow properties. Concurrently, the snow ablation processes

in continuous forest, a forest glade, and on grassland were systematically observed by snow depth and snow density measurement to evaluate the “forest effects” on the processes of snow accumulation and ablation.

Materials and methods

Study site

The Kuwei snow station was established on the southern slope of middle Altai Mountains in August 2011 to study snow, frozen soil, snow and permafrost hydrology, and their interactions with each other and climate change. The Kuwei station (47°21'9.1"N, 89°39'43.22"E; 1379 m a.s.l.) is located in the Kayiertesi River Basin, the first level branch of the Irtysh River (Fig. 1), 27 km from the town of Koktokay, also known as the “second cold pole of China”. The area of Kayiertesi River Basin is approximately 2365 km² and the altitude ranges from 1341 to 3846 m. The bedrock is widely exposed. Generally, the soil layer is relatively thin and the soil type is classified as sandy soil. An organic soil layer is widely distributed in the north facing slopes and valley plain and its depths are about

10–40 cm. Basin-wide survey results in August 2014 indicated that permafrost was not frequent because of the thin soil layer, except in the river valley, and the lowest altitude where permafrost could form was about 1700 m a.s.l.

The vegetation is rich in the study basin and the forest cover ratio is 39.2 % in 2014. The tree line was 2300–2400 m a.s.l. in the north facing slope and at 2050–2150 m a.s.l. in the sunny slope. The land surface is generally covered by forest in the shade and semi-shade and is captured by grassland and shrubs in the sunny and semi-sunny slopes. Shrubs are mainly distributed below 2000 m a.s.l. The dominant tree species are *Abies sibirica* and *Larix sibirica* wood. The whole basin is controlled by west winds. The average annual precipitation monitored by Kuwei hydrological station from 1979 to 2013 is about 360 mm, and the precipitation type was usually snowfall from November to April of the next year. The basin is usually covered by snow over 5 months from November onward, and the snow can last until June in the high-altitude region. Flood processes are caused by simultaneous snowmelt and rainfall and always occur in May, June, and July. During 1956–2014, the maximum instantaneous discharge was about 498 m³ s⁻¹ in May 29, 1969 and mean

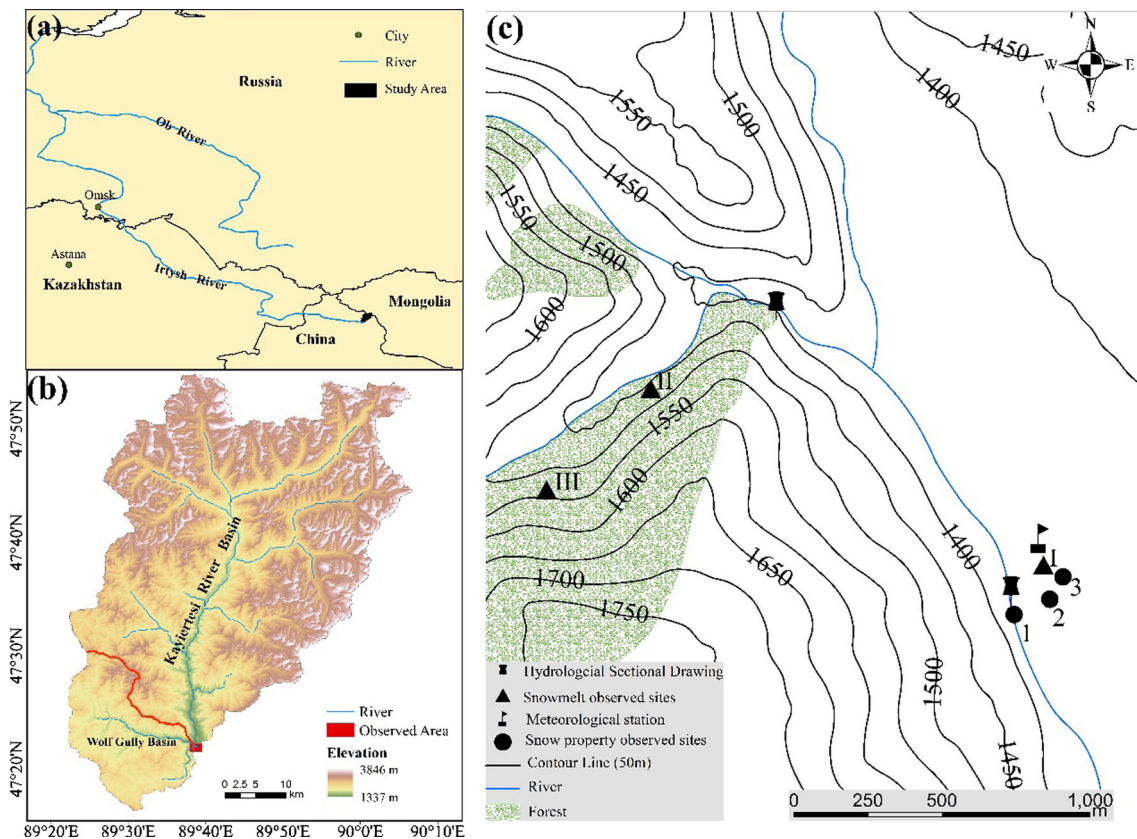


Fig. 1 Maps showing the study region and distributions of observed sites. In *c* dots 1, 2, and 3 denote river ice, concrete and grassland; triangles I, II, and III denote grassland, forest glade and continuous forest, respectively

maximum monthly discharge was approximately $100 \text{ m}^3 \text{ s}^{-1}$ in June.

Field measurements and methods

Meteorological data were collected by an automatic meteorological station from August 15, 2011 on. The snow depth and snow water equivalent (SWE) were measured by snow pillow and SR50A Sonic Ranging Sensor (Campbell Scientific, USA), respectively. Snow temperature probes were installed at 10, 15, 20, 30, and 40 from the ground surface. Soil temperature and water content sensors were likewise fixed at 5, 10, 20, 40, 60, 80, 120, 160, 200, and 250 depths. Two soil heat flux sensors were placed horizontally at 5 cm depths. Land/snow surface temperature was monitored by an SI-111 Precision Infrared Radiometer Sensor (Campbell Scientific, USA). All the sensors were connected to one CR3000 data logger (Campbell Scientific, USA) and the data recording interval was 30 min. The main sensors and resolution are shown in Table 1.

The snow physical properties and snowmelt processes were monitored during the snowmelt period in 2014. Snow layer temperatures, LWCs, and density of snow cover on the grassland, river ice, and concrete were acquired. The thickness of the river ice was about 110 cm and the water depth under the river ice was ~ 70 cm. The concrete ground was built in 2010 and the thickness was about 13 cm. A Finnish Snow Fork was utilized to measure the layered snow density and LWC. The measurements began from the snow surface and sampling was carried out at 5-cm intervals until the bottom of the snow cover was reached. Data from two snow pits on the same underlying surface were collected every day at 07:00, 10:00, 12:00, 15:00, and 17:00 local time in the Chinese Altai Mountains (GMT + 6.0). The snow temperature was measured by a TP3001 portable thermometer (accuracy ± 0.5 °C,

measurement range -50 to 300 °C) at 07:00, 12:00, and 17:00 from March 18 to 22. The snow pits were slightly dug out before each measurement.

Three land use patterns were selected to investigate the snowmelt processes: grassland, continuous forest, and forest glade (Table 2). The grassland and forest glade were flat, but the forest had a slope $< 5^\circ$. The forest consisted of *A. sibirica* and the tree height was approximately 30 m. The forest glade was nearly circular with a diameter of 30 m and was surrounded by ~ 30 -m *A. sibirica*. The snowmelt processes were analyzed using more than 20 snow stakes uniformly distributed at each observation site. For example, five snow stakes, Nos. 18–22[#], were installed southeast of one single tree on the edge of forest (Fig. 2). The snow stakes on the grassland were read at 07:00, 12:00, and 17:00, but those in the continuous forest and forest glade were measured only once per day between 08:30 and 09:00. The air temperature (accuracy ± 0.2 °C) and relative humidity (accuracy ± 2.5 %) were collected by a HOBO Pro V2 (Onset Computer Corp., USA) at 10-min intervals.

In this study, one new parameter, diurnal ablation percentage (DAP), was used and defined as follows:

$$\text{DAP} = Q_t / Q_w \times 100 \%$$

where Q_w is the daily total of snowmelt whereas Q_t is the ablation during a specific sub-daily period. The units are mm.

Results and discussions

Meteorological conditions

Several meteorological variables that were recorded by an automatic meteorological station during the snow melt

Table 1 Main instruments and their properties at the Kuwei station

Observation items	Sensor	Resolution	Ranges of utilization	Observation accuracies
Air temperature	1000 Ω PRT, IEC 751 1/3 Class B	0.1 °C	-40 to 60 °C	± 0.4 °C
Relative humidity	HUMICAP ^R 180	1 %	0 to 100 %	2 %
Wind speed	05103 Young wind monitors	0.1 m/s	0 to 100 m/s	± 0.3 m/s or 1 %
Wind direction	05103 Young wind monitors	1°	0 to 360°	$\pm 5^\circ$
Precipitation	TRwS 500/TRwS503	0.1 mm	0 to 60 mm/min	0.1 % FS
Solar radiation	CNR4	–	-40 to 80 °C	1 %
Snow depth	SR50A	0.25 mm	0.5 to 10 m	± 1.0 cm or ± 0.4 %
Land/snow surface temperature	SI-111	0.1 °C	-40 to 70 °C	± 0.5 °C
Snow layered temperature	BetaTherm 10K3A1 Thermistor	0.1 °C	-50 to 70 °C	± 0.5 °C
Soil temperature	Hydra	0.1 °C	-30 to 65 °C	± 0.1 °C
Soil water content	CS616/CS625	0.10 %	0 to 100 %	± 0.1 %
Soil thermal flux	Thermopile	50 $\mu\text{V/W/m}^2$	± 2000 W/m ²	± 5 %

Table 2 Detailed informations in three snowmelt observed sites

Observation sites	Longitude	Latitude	Altitude (m)	Snow stake numbers	Observation periods	Observation times
Grassland	47°21'09.10"N	89°39'43.22"E	1379	20	March 7–25	07:00, 12:00, 17:00
Forest glade	47°21'33.46"N	89°39'43.92"E	1410	22	March 8 to April 20	08:30
Continuous forest	47°21'24.19"N	89°38'30.23"E	1432	23	March 9 to April 13	08:50

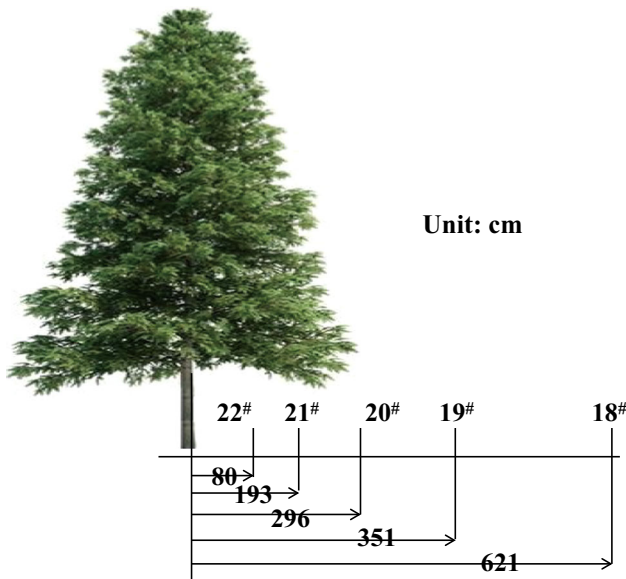


Fig. 2 Conceptual graph showing the distribution of five snow stakes in the southeastern direction of one single tree on the edge of forest in the continuous forest cover region

period in 2014 are shown in Fig. 3a. Overall, the precipitation was dominated by snow events in March, sleet in early-mid April, and rain in late April. Two significant snowfalls occurred, on March 9 and 15. The increases in snow depth were 12.7 and 2.9 cm, respectively, and the new snow densities were 92.9 and 89.7 kg m⁻³. The daily mean snow surface temperature was always lower than the air temperature during that period.

Diurnal variations of air temperature and diurnal temperature ranges (DTRs) from March 10 to 24 were assessed (Fig. 3b, c). The mean air temperatures were -2.5 °C on the grassland, -5.4 °C in the continuous forest, and -6.1 °C in the forest glade. The air temperature recordings coincided well and the diurnal variations of air temperature indicated that the air temperature in the grassland was always higher than in the forest regions during the survey period (Fig. 3b). The significant interception of downwelling shortwave radiation by the canopy (Pomeroy et al. 2008) resulted in the air temperature being the highest on the grassland and lowest in the forest glade. In addition, the differences of the temperature field were reflected in the DTRs (Fig. 3c), which

indicated that the DTR in the continuous forest was the smallest of the three underlying surfaces, except for the snowfall processes on March 15. The mean DTRs were 14.2 °C on the grassland, 15.0 °C in the forest glade and 11.6 °C in the continuous forest.

Snow temperature

Diurnal variations of the surface snow temperature on the concrete, river ice and grassland were consistent with each other (Fig. 4a) and had good correlations with air temperature, which was relatively homogeneous. The bottom snow temperatures measured at the same times from March 18 through 23 were averaged and are shown in Fig. 4b. Overall, the diurnal variations displayed a unimodal style on the river ice and grassland, and the temperature was highest in the afternoon. However, the temperature exhibited a bimodal style on the concrete, which first slowly decreased from 07:00 to 12:00, then increased until 17:00, and then quickly declined. The maximum temperatures occurred at 07:00 (or earlier) and 17:00 on the concrete structure. Meltwater refreezing might be the main reason that caused snow temperature variations at the bottom layer on the concrete. In our field investigation, one ice layer was discovered between the concrete and snow layer in the morning. But at noon, the ice layer disappeared. It is therefore suspected that the decline in temperature is related to ice melt on the concrete surface. In the morning, the snow temperature at the bottom would increase due to energy input from surface layer if there was no ice layer. However, because of energy consumption required for melting this ice layer, the snow temperature displayed a declining trend. Further observations are still needed to study these phenomena more thoroughly. Moreover, compared with the surface snow temperature, diurnal variations in the bottom snow temperature were more moderate.

The vertical temperature profiles on the three underlying surfaces (Fig. 4c) demonstrated that the vertical variation of the snow temperature on the grassland was generally coincident with the vertical variation on the concrete, but was different from the vertical variation on the river ice. The temperature of the middle layer was always largest on the grassland and the concrete, but it had a fluctuant rising trend with deeper depths on the river ice, where the

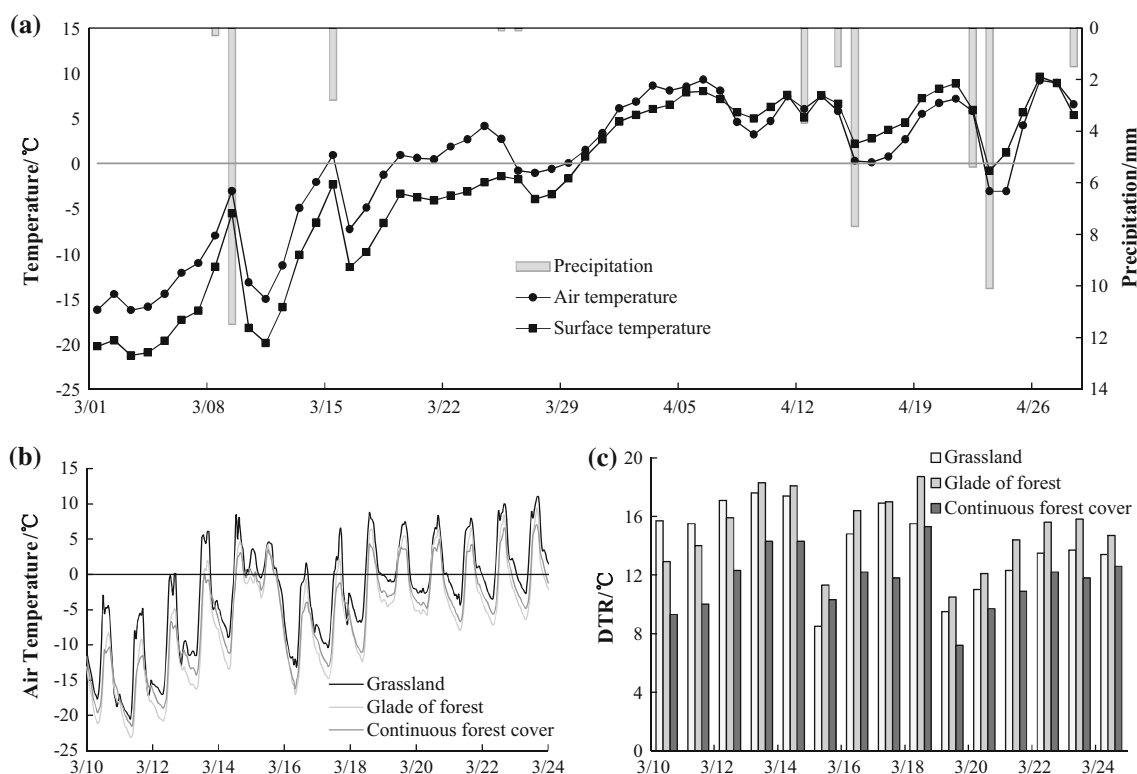


Fig. 3 **a** Daily precipitation and air temperature observed by automatic meteorological station at Kuwei station from March 1 to April 28, and **b** hourly air temperature, **c** DTR on grassland, forest glade forest and continuous forest

minimum temperature was at the surface and the middle of the snow cover.

Snow LWC

In terms of LWC, snow is classified by IAHA (International Association of Scientific Hydrology) as dry ($LWC = 0\%$), moist ($LWC < 3\%$), wet ($3 < LWC < 8\%$), very wet ($8 < LWC < 15\%$), and slush ($LWC > 15\%$) (Colbeck et al. 1990). In this study, scarcely any liquid water was discovered in the whole snow layer before March 15. Therefore, before March 15, 2014 in the Altai Mountains, the snow was classified as dry snow.

The mean LWC at one certain moment or depth was obtained by averaging the LWCs at that moment or depth from March 15 to 22. The same diurnal variation trends of LWC of the surface snow layer were demonstrated on the concrete, river ice, and grassland (Fig. 4d), and they markedly correlated with, but slightly lagged snow surface temperature (Fig. 4e). The LWC changes in the bottom snow were quite different from each other on the three underlying surfaces, but liquid water existed in the daytime on all of them. There was no significant diurnal change in the LWCs on the river ice, which stably fluctuated around

0.5 %. The bottom snow LWCs on the grassland were usually higher than on the river ice, and ranged from 1.2 % at 10:00 to 2.4 % at 17:00. But, the diurnal range of the bottom snow LWC on the concrete was relatively large; a rapid increase in LWC from 1.5 % at 12:00 to 4.0 % at 15:00 was captured.

Overall, the mean LWCs of the whole snow cover in the daytime from March 15 to 22 were 1.12 % on concrete, 0.39 % on river ice, and 1.27 % on grassland. Based on the LWC, the snow was classified as moist snow during the strong snowmelt period. The vertical profiles of LWCs on three underlying surfaces are illustrated in Fig. 4f. The LWCs in the middle snow layer (from 10 to 20 cm) were always smaller than in the surface and bottom snow layers (Fig. 4f); the limited depth affected by ambient solar radiation and atmospheric temperature (Chen et al. 2011) might be the main reason. The LWCs fluctuated with the smallest amplitude below 0.5 % from the surface to the bottom on the river ice, although the snow cover there was the thickest. The LWC range on the concrete was the greatest, from 0.3 to 2.3 %. The peak LWCs were found at the bottom of the snow cover on the concrete and the grassland. The bottom LWC was relatively low on the river ice and there was an approximately 10 cm-deep hoar layer in the bottom snow layer because liquid water had

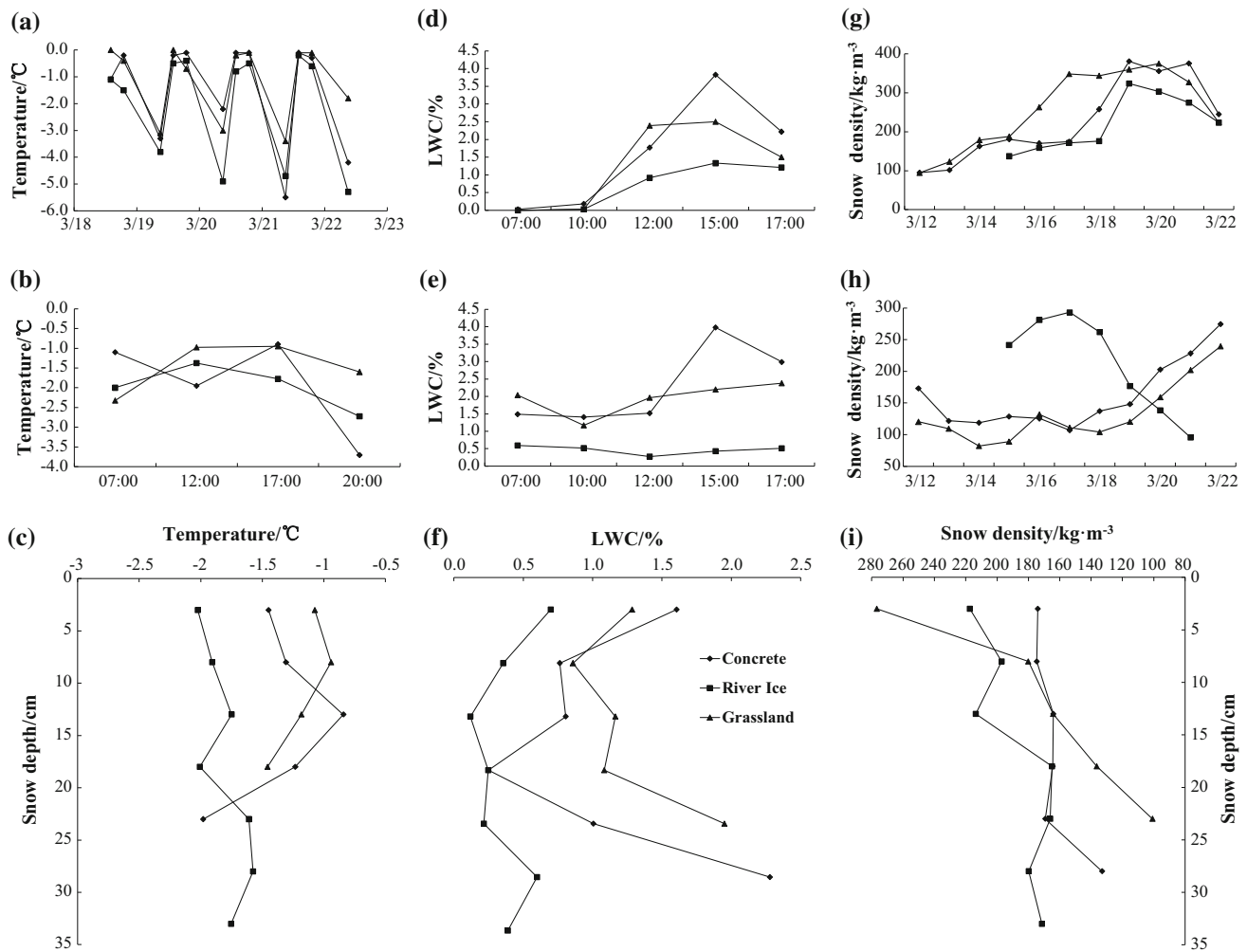


Fig. 4 Variations in snow temperature, LWC and snow density. **a, d, g** represented temperature, LWC, density of surface snow layer from 0 to 5 cm; **b, e, h** represented temperature, LWC, density of bottom

snow layer; **c, f, i** represented vertical profiles of snow temperature, LWC and density

separated out from the snow cover and then refroze on the surface of the river ice, which was similar to the conglation formation of the sea ice (Maksym and Jeffries 2000) and ice in mountain glaciers (Cuffey and Paterson 2010).

Synchronous datasets (171 pairs) of temperatures and LWCs recorded at 07:00, 12:00, and 17:00 from March 18 to 22 were utilized to explore the relationship between the snow temperature and LWC. The LWCs of half of the samples (85) equaled 0 (Fig. 5a), and only one sample was discovered in which the LWC was more than 6%. A scatter diagram of snow temperature and LWC (Fig. 5b) showed during the snowmelt period in the Altai Mountains the snow temperature ranged from -5.5 to 0.0 °C and the LWC ranged from 0 to 6.2%. Commonly, the LWC increased with rising temperature, but there was no regular increasing trend.

As one less-than-ideal alternative method, the LWC could be classified into three categories according to the

snow temperature. When the snow temperature was below -2.5 °C, the LWC always equaled 0 and the liquid water in the snow cover could be neglected. When the snow temperature rose, but still remained below -1 °C, the liquid water content of more than 43.3% of the samples was below 1%. With a continuous increase in snow temperature, that is, when the snow temperature exceeded -1 °C, the liquid water rapidly increased and 67 of the samples (65.7%) contained liquid water. In addition, the LWC randomly fluctuated within the range from 0 to 6.2%.

Snow density

The daily mean snow density was obtained by averaging measured snow densities at 07:00, 10:00, 12:00, 15:00, and 17:00. The surface snow density from the 0–5 cm depth gradually increased before March 15 and the densification

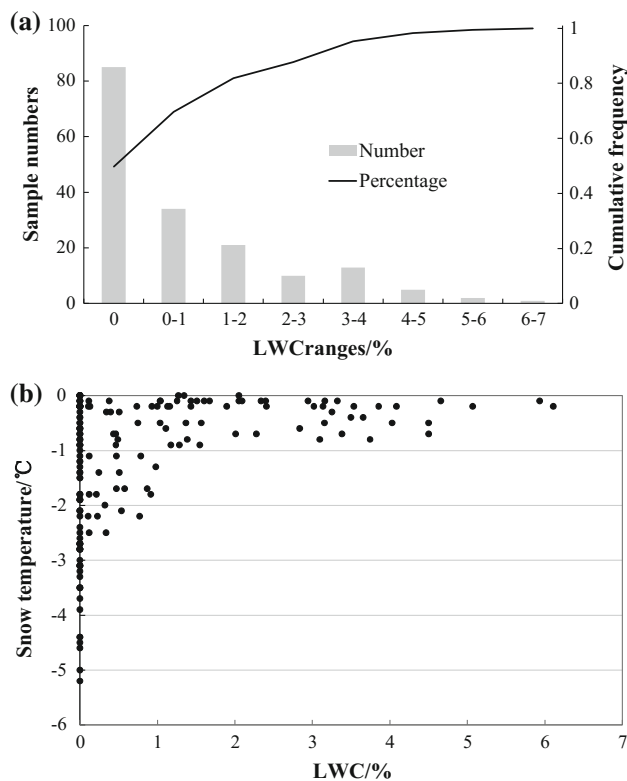


Fig. 5 Statistic results of LWC derived from Snow Fork (a) and relationships between snow LWC and temperature (b) during the snow melt period

accelerated during March 16–20 because of snowmelt, and then the density began to decrease on all three underlying surfaces (Fig. 4g). The daily mean snow density varied stably and slightly decreased before March 18 at the contact surfaces between the snow cover and the concrete and the grassland (Fig. 4h). Then, rapidly increasing linear trends in the bottom snow density appeared from March 19 to 22; the gradients were $33.3 \text{ kg m}^{-3} \text{ d}^{-1}$ ($R^2 = 0.975$) on the concrete and $35.2 \text{ kg m}^{-3} \text{ d}^{-1}$ ($R^2 = 0.982$) on the grassland. Change of bottom snow density on the river ice was not in agreement with the variations on the concrete and grassland. The bottom snow on the river ice densified before March 17, but the snow density had a rapid linear decline with a gradient of $-51.9 \text{ kg m}^{-3} \text{ d}^{-1}$ ($R^2 = 0.978$) from March 17 to 22 on the river ice.

The vertical profiles of snow density are shown in Fig. 4i and the densities are the mean values from March 12 to 22 on the concrete and grassland, but from March 15 to 22 on the river ice. The snow densities of the surface layers were greatest on all three underlying surfaces. Vertical changes were relatively moderate from the surface to the bottom on the river ice and concrete, ranging from 165.0 to 217.3 kg m^{-3} and from 174.6 to 132.9 kg m^{-3} , respectively. But, an abrupt decline in snow density was observed on the grassland, which decreased from

276.7 kg m^{-3} in the surface layer to 100.8 kg m^{-3} at the bottom within a 30 cm depth snow because of the water storage property of the withered grass layer. Overall, we could discover that vertical variation ranges of snow densities on the river ice (52.3 kg m^{-3}) and concrete (41.7 kg m^{-3}) were relatively less than that on the grassland (175.9 kg m^{-3}), although the snow cover on the grassland was the shallowest. So we concluded that the snow cover on the river ice and concrete was more homogeneous than that on the grassland.

Snowmelt processes

Variations of snow depth and SWE were monitored by a snow pillow, and showed that the SWE variation was not consistent with the snow depth (Fig. 6a). The ongoing decrease in snow depth was persistent from March 10, until it disappeared; snow depth declined about 9.4 cm from March 10 to 18. However, the SWE was approximately constant during the same period, aside from a slight increase caused by snowfall on March 15. Quick decreases in SWE, with a gradient of 10.7 mm d^{-1} , were confirmed from March 21 to 24 when the daily mean air temperature was above $0 \text{ }^\circ\text{C}$ from March 19 onward (Fig. 3).

The snow cover mainly consisted of two parts: an old snow layer (snowfall on January 30 and 31) and a new snow layer (snowfall on March 9). To explore which part led to the difference of snow depths and SWE variations, the depth and density of the new snow layer were analyzed (Fig. 6b). The results illustrated that the depth of the new snow layer quickly decreased from 11.8 cm on March 9 to 4.5 cm on March 15 and the snow density increased from below 100 kg m^{-3} to over 250 kg m^{-3} . The new snow depth decreased by 7.3 cm, nearly 78 % of the decrease in the whole snow cover.

In this study, the snowmelt and runoff data sets were used to calculate the concentration time. For the convenience of statistical analysis, daily snowmelt cycles were set to begin at 17:00. Diurnal snowmelt processes were artificially divided into three intervals: from 17:00 to 07:00 of next day (Interval A), from 07:00 to 12:00 (Interval B), and from 12:00 to 17:00 (Interval C). The detailed diurnal ablation percentage (DAP) variations of the three Intervals are shown in Fig. 6c. Generally, eliminating the effect of the snowfall event on March 15, the intensive snowmelt occurred in Interval C, when the snowmelt amount was more than 50 % and the maximum DAP was 83 % on March 18. With continuous snowmelt, the DAP in Interval C gradually declined, but it increased in Interval A and B from March 18 until the end. In March, April, and May the diurnal maximum discharge occurred at night, between 23:00 and 01:00 (P1) in Kayiertesi river basin. In summary, the snowmelt mainly happened in Interval C and daily

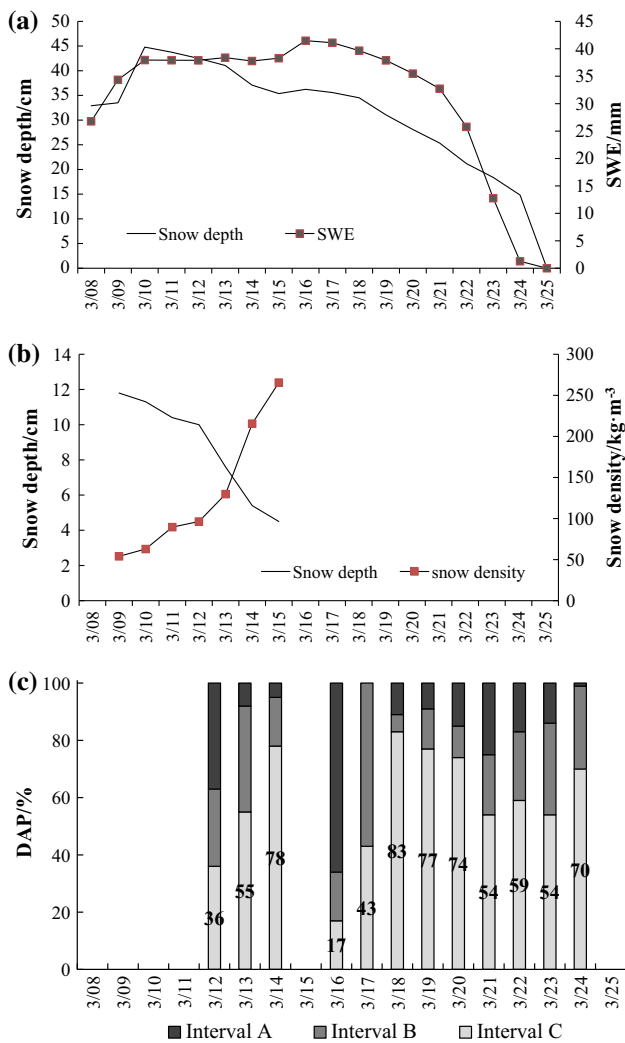


Fig. 6 Variations of snow depth and SWE on snow pillow (a), depth and density evolutions (b) of new snow layer formed on March 9 and DAP variations (c) during the snow melt period on the grassland

maxima of streamflow occurred in the period from 23:00 to 1:00 of the next day. The median values of Section C and P1 were chosen as the representative points for maximum snowmelt and discharge, respectively. The time of confluence was the difference between these points in time. Then, the time of confluence was roughly deduced and was approximated as 9.5 ± 3.5 h for the Kayiertesi River Basin.

Forest effects on snow melt

Two observation sites in the windward forest, the continuous forest and the forest glade, were located on same windward slope and were only a few hundred meters apart from each other. The differences of snow accumulation were only attributed to the forest cover. The SWEs were 61.6 mm in the forest glade and 43.5 mm in the continuous

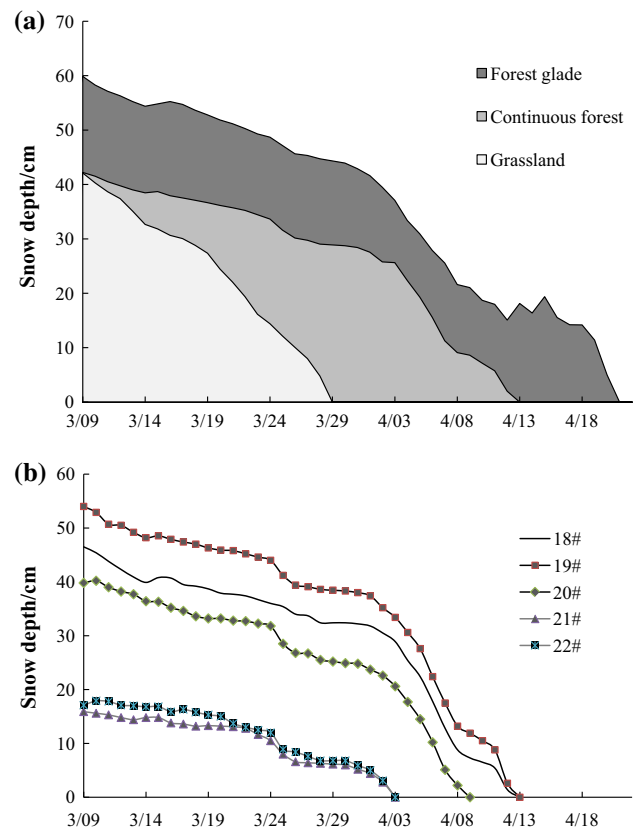


Fig. 7 Snow depth and SWE variations during the snowmelt period: a daily variations of snow depths at three observation sites; b variations of daily snow depths at five monitored points in the southeast of one single tree of *A. sibirica* on the edge of continuous forest

forest on March 9. Regardless of the variation in snow cover before March 9, the average snow interception rate by *A. sibirica* trees was 29.4 %.

Variations of daily average snow depths on the three different surfaces are shown in Fig. 7a. The end date of the snowmelt was March 29 on the grassland, 15 days earlier than in the continuous forest and 23 days earlier than in the forest glade. According to snow depth and SWE variations measured with the snow pillow (Fig. 6a), the snowmelt period was artificially defined to begin on March 10. Then the snowmelt period was easily obtained and it was 20 days on the grassland, 35 days in the continuous forest, and 43 days in the forest glade. The average snowmelt rates were calculated by the SWE on March 10 dividing snowmelt periods, and were 2.1 mm d⁻¹ on the grassland, 1.5 mm d⁻¹ in the forest glade, and 1.2 mm d⁻¹ in the continuous forest. Furthermore, the day degree factors (DDFs) during the whole snowmelt period on the grassland, in the continuous forest, and forest glade were calculated according to the equation provided by Hock (2003). The relative variables (snow depth and snow density) of calculating DDF were obtained from direct measurement

using ablation stake method. The total ablation amount was monitored by snow stakes (snow depth) and Snow Fork (snow density), and the temperature was synchronously measured by Hobo. The calculated result showed that the DDF on the grassland ($2.46 \text{ mm d}^{-1} \text{ }^{\circ}\text{C}^{-1}$) was twice more than those in the continuous forest ($1.07 \text{ mm d}^{-1} \text{ }^{\circ}\text{C}^{-1}$), and forest glade ($1.27 \text{ mm d}^{-1} \text{ }^{\circ}\text{C}^{-1}$). In addition, the unobvious difference of DDFs between the continuous forest and forest glade was because of small air temperature difference.

To explore the dependency between snowmelt processes and air temperature, and solar radiation, the daily snowmelt rates in the three different surfaces were calculated and are shown in Fig. 8. Then the snowmelt period was divided into cold and warm periods according to the daily air temperature: the cold period was when the daily mean air temperature remained below $0 \text{ }^{\circ}\text{C}$ and the warm period was when the daily mean air temperature was always above $0 \text{ }^{\circ}\text{C}$. Mean air temperatures and SMRs were calculated in the cold and warm periods, respectively, and the statistical results are shown in Table 3. The results indicate that the maximum SMRs, 5.4 mm d^{-1} on the grassland, 6.3 mm d^{-1} in the forest glade, and 6.2 mm d^{-1} in the continuous forest, were not significantly different during the overall snowmelt period. The SMR relationships in the three surfaces were different in the cold and warm periods, although air temperature departures with different land use types were little difference in both cold and warm period. In the cold period, the mean air temperatures were $-5.7 \text{ }^{\circ}\text{C}$ on the grassland, $-6.4 \text{ }^{\circ}\text{C}$ in the forest glade, and $-6.3 \text{ }^{\circ}\text{C}$ in the continuous forest, but the SMR in the forest was much smaller than on the grassland and in the glade. However, the SMRs were similar on the three surfaces in the warm period, although the same differences of air temperature under the three surface conditions still existed.

From a statistical standpoint, the SMR could be described by only the sum of the positive air temperature or the synergy of air temperature and the shortwave radiation balance or net radiation (Hock 2003). The above results indicate that, to a certain degree, the SMR might be more sensitive to radiation in cold periods because, as discussed by Pomeroy et al. (2008), the absorbed solar radiation in the continuous forest sub-canopy was less than half that of the top canopy when cloud cover was neglected, but the air temperatures were similar (Fig. 3; Table 3). When the daily mean air temperature was above $0 \text{ }^{\circ}\text{C}$ and lasted, the SMR was mainly controlled and described by the air temperature. The SMR in the forest was slightly greater than in the forest glade because of the slightly higher air temperature (only $+0.1 \text{ }^{\circ}\text{C}$), in spite of more absorbed radiation in the forest glade. However, the SMRs alters sharply day by day when the average temperature is $>0 \text{ }^{\circ}\text{C}$.

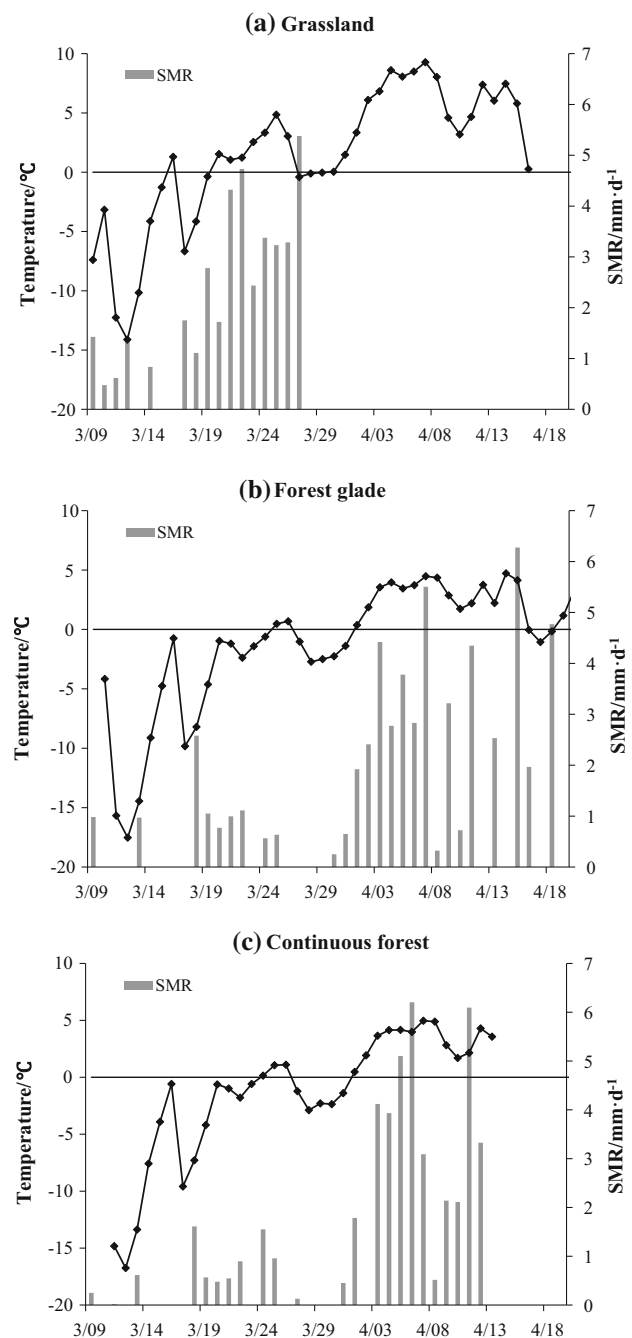


Fig. 8 Relationships of SMRs and daily average air temperature during the snowmelt period at three observation sites. Negative values are not shown

It may be caused by the following two factors: on the one hand, the snowmelt will accelerate with continuous energy input. Given that the energy input is equal, a snow pack (or snow layer) with higher temperature is subjected to higher melt rates than a snow pack with lower temperature. In the latter case, a greater fraction of available energy is initially required to raise the temperature of the snow pack to $0 \text{ }^{\circ}\text{C}$. On the other hand, the snow properties will change in the

Table 3 Statistical results of average air temperature and SMRs in both cold and warm periods

	Cold period				Warm period			
	Dates	Temperature (°)	Solar radiation (W m ⁻²)	SMR (mm d ⁻¹)	Dates	Temperature (°)	Solar radiation (W m ⁻²)	SMR (mm d ⁻¹)
Grassland	Mar 09–19	-5.7	204.7	1	Mar 20–26	2.5	204.2	3.3
Forest glade	Mar 09–24	-6.4	–	0.6	Apr 01–15	3.2	–	3.2
Continuous forest	Mar 09–23	-6.3	–	0.3	Apr 01–12	3.3	–	3.5

snowmelt processes, such as decline in snow albedo, which will affect the energy balance in the snow surface.

Therefore, our conclusion is concisely summarized as that the SMR was described by the air temperature and radiation when the daily mean air temperature was below 0 °C; however, when the daily mean air temperature lasted above 0 °C, the SMR was calculated by only using air temperature. Because of deficiencies of radiation in the glade and the sub-canopy forest, only the qualitative conclusion on the relationship between SMR and air temperature and radiation is given here. However, this discovery was beneficial for further understanding and improving the snowmelt degree day factor algorithm.

Effect of a single tree on snow accumulation and ablation

Snow stakes numbered 18[#] through 22[#] were installed southeast of a single *A. sibirica* tree (Fig. 2) on the edge of the continuous forest, to monitor the variations of snow depth. The snow depth measurements are shown in Fig. 7b. Given the different distances from the tree trunk, the snow depths were highly non-uniform, ranging from 15.9 cm at stake 21[#] beneath the sub-canopy to 54 cm at stake 19[#] outside the canopy. On the basis of the snow depth in the glade (60 cm), the snow interception rates at the five measurement points (stakes 18[#] through 22[#]) were roughly computed and the values were 22.5, 10, 33.7, 73.5, and 71.5 %, respectively. Then the snow measurement points were roughly divided into three types: in the sub-canopy (21[#] and 22[#]), on the edge of the canopy (20[#]), and outside of the canopy (18[#] and 19[#]). The snowfall interception rates above the sub-canopy observation, were the largest, over 70 %, followed by the edge of the canopy (33.7 %), and outside of the canopy (only 10 to 22.5 %). The snow cover mainly formed on January 30–31 and March 9, and the amount of precipitation and average wind speeds during the snowfall period were 24.0 mm and 0.49 m s⁻¹, and 11.8 mm and 0.28 m s⁻¹, respectively. On the one hand, the wind speed was slow when snow fell. Snow cover was shallow in the sub-canopy due to strong snowfall interception by the tree crown. Therefore, snow depths in the sub-canopy were

less than at the edge and outside of the canopy. On the other hand, the snow intercepted by the canopy was another significant source of snow after the snowfall because prevailing winds from the northwest contributed to snow accumulation to the southeast, outside of the canopy, which was consistent with the result by Revuelto et al. (2015). Therefore, the amount of snow accumulation was highest outside of the canopy and was the least in the sub-canopy.

That single tree also had a significant effect on snow ablation. The snow cover in the sub-canopy first disappeared on April 3. The end of snow ablation on the edge of the canopy lagged 6 days and occurred on April 9. Finally, the snow cover outside of the canopy vanished on April 13. The snowmelt periods were 25 days in the sub-canopy, 31 days on the edge of the canopy, and 35 days outside of the canopy. The mean variation rate of snow depth was calculated by having the initial snow depth on March 10 dividing the time interval from snowmelt beginning to the end; the mean ablation rates at measurement points 18[#] through 22[#] were 1.3, 1.5, 1.2, 0.6, and 0.7 cm d⁻¹, respectively. The average snow ablation rates were 1.4 cm d⁻¹ outside of the canopy, 1.2 cm d⁻¹ on the edge of the canopy, and 0.6 cm d⁻¹ in the sub-canopy. Regardless of the snow density differences, the snow ablation rate outside of the canopy was more than twice that in the sub-canopy.

How the forest affects snow accumulation and ablation processes is still problematic. Relevant researches on mathematical descriptions of forest cover in numerical models have focused on parameterization schemes of snowfall interception and radiation transport in forest canopies (Andreadis et al. 2009; Mohammed and Tarboton 2014; Pomeroy et al. 2012; Varhola et al. 2010). The development of a forest cover parameterization scheme is a significant way to improve snow hydrological simulation when the forest cover is not ignorable. However, this current field experiment in the headwater region of Irtysh River was relatively simple. The existing data sets cannot be used to support our further study, so subsequent field observations will be designed to assess in detail the impact of forest cover and single trees on snow accumulation and ablation, and on snow hydrology.

Conclusions

The temperature field and thermal properties of an underlying surface have a significant impact on the physical properties of an overlying snow cover, especially the bottom snow layer. On the one hand, the temperature field of the underlying surface affects the snow temperature of the bottom layer; we found a lower diurnal temperature range in the bottom snow layer on river ice, which was attributable to the relatively constant temperature of the river water below the river ice. On the other hand, thermal properties such as the higher heat conductivity of concrete can lead to a faster temperature change rate and larger temperature diurnal range in the bottom snow layer on the concrete. In addition, the potential feedback of the snow cover to the underlying surface is not negligible. We found that meltwater refreezing on the river ice surface made a significant contribution to the growth and development of river ice.

Diurnal variation patterns in snow temperature and the LWCs of surface snow layers were consistent with each other on the three studied underlying surfaces. In the bottom snow layer, diurnal variations of snow temperature showed a unimodal variation pattern on the grassland and river ice surfaces, but a bimodal variation pattern on the concrete surface. Mean snow temperatures in the middle snow layer were highest on the grassland and concrete, but snow temperature variations increased from the surface to the bottom on the river ice. The diurnal LWC range at the bottom of the snow cover on the grassland was less than that on the concrete, and decreased further on the river ice. The mean LWC in the middle snow layer was the smallest on three underlying surfaces. The maximum LWC presented in the bottom snow layer on the grassland and concrete. However, the bottom LWC on the river ice was relatively low and the surface LWC was largest. Overall, the LWC increased with higher snow temperature: it was equal to zero when the snow temperature was below $-3\text{ }^{\circ}\text{C}$; it slightly increased, but was still below 1 % when the snow temperature varied from -3 to $-1\text{ }^{\circ}\text{C}$, and it quickly increased when the snow temperature was above $-1\text{ }^{\circ}\text{C}$. Rapid increases in the mean snow density during the early snow melt period and in the bottom snow density during the late snowmelt period were discovered on the grassland and concrete; however, a fast decline in bottom snow density at a rate of $-51.9\text{ kg m}^{-3}\text{ d}^{-1}$ from March 17 to 22 was observed because surface snow melted and flowed through the snow cover by percolation and then the meltwater refroze on the river ice surface.

Overall, both continuous forest and single trees have significant impacts on snow accumulation and ablation.

First, a forest has the ability to affect the air temperature. Both the mean daily temperature and the diurnal temperature range in the forest were lower than in the open grassland, but the mean daily air temperature in the sub-canopy was consistent with that of the corresponding forest glade. The snow depth in the continuous forest was much less than in the adjacent open field and approximately 30 % of the snowfall was intercepted by the canopy. For one single tree, however, the snowfall interception rate varied from more than 70 % beneath the canopy, to 34 % on the edge of the canopy, to 10 % outside of the canopy. The last date of snow ablation in the studied forest was much later than that on the grassland. The remaining period of snowmelt on the grassland was 20 days, which was half that in the forest. The duration of snow ablation beneath the canopy was slightly shorter than that on the edge and outside of the canopy due to smaller snow accumulation. The mean SMR in the glade (1.5 mm d^{-1}) was larger than that in the continuous forest region (1.2 mm d^{-1}), but was much less than that on the grassland (2.1 mm d^{-1}). The SMR outside of the canopy was consistent with that on the edge, but was twice that beneath the canopy. It is worth noting that the SMR was sensitive to solar radiation when the mean air temperature was below $0\text{ }^{\circ}\text{C}$, but more sensitive to air temperature when the mean air temperature persistently exceeded $0\text{ }^{\circ}\text{C}$. Additionally, the fact that the confluence time of snowmelt discharge in the Kayiertes River Basin was approximately $9.5 \pm 3.5\text{ h}$ was encouraging for accurate further forecasts of snow hydrology in the Irtysh River Basin.

Acknowledgments This work was supported in part by the National Natural Science Foundation of China (Grant Nos. 41190084, 41271083, 41201062), State Key Laboratory of Frozen Soil, Cold and Arid Regions Environmental and Engineering Research Institute, Chinese Academy of Sciences (Grant Number: SKLFS201412), and the Special Talent Exhume Project (J1210003/J0109). Thanks are given to the editors and two anonymous reviewers for their valuable suggestions for enriching the content and presentation, and Anda Divine (Editorial staff in Sciences in Cold and Arid regions) from USA for substantially improving the English and good suggestions. We also acknowledge the field staff of the Kuwei National Basic Hydrological Station, Bin He and Feng Diao, for their assistance in field data collection.

References

- Andreadis KM, Storck P, Lettenmaier DP (2009) Modeling snow accumulation and ablation processes in forested environments. *Water Resour Res* 45. doi:Artn W05429
- Avanzi F, Caruso M, Jommi C, De Michele C, Ghezzi A (2014) Continuous-time monitoring of liquid water content in snow-packs using capacitance probes: a preliminary feasibility study. *Adv Water Resour* 68:32–41

- Barnett TP, Adam JC, Lettenmaier DP (2005) Potential impacts of a warming climate on water availability in snow-dominated regions. *Nature* 438:303–309
- Bartels-Rausch T et al (2014) A review of air-ice chemical and physical interactions (AICI): liquids, quasi-liquids, and solids in snow. *Atmos Chem Phys* 14:1587–1633
- Bormann KJ, Westra S, Evans JP, McCabe MF (2013) Spatial and temporal variability in seasonal snow density. *J Hydrol* 484:63–73
- Brown RD, Robinson DA (2011) Northern Hemisphere spring snow cover variability and change over 1922–2010 including an assessment of uncertainty. *Cryosphere* 5:219–229
- Burns SP et al (2013) Snow temperature changes within a seasonal snowpack and their relationship to turbulent fluxes of sensible and latent heat. *J Hydrometeorol* 15:117–142
- Chen X, Wei W, Liu M, Gu G (2011) Variations of snow temperature and their influence on snow cover physical parameters in the Western Tianshan Mountains, China. *J Mt Sci* 8:827–837
- Colbeck S et al. (1990) The international classification for seasonal snow on the ground. The international commission on snow and ice of the international association of scientific hydrology
- Cuffey KM, Paterson WSB (2010) *The physics of glaciers*, 4th edn. Butterworth-Heinemann, Burlington
- Essery R et al (2008) Radiative transfer modeling of a coniferous canopy characterized by airborne remote sensing. *J Hydrometeorol* 9:228–241
- Essery R, Morin S, Lejeune Y, Menard CB (2013) A comparison of 1701 snow models using observations from an alpine site. *Adv Water Resour* 55:131–148
- Hock R (2003) Temperature index melt modelling in mountain areas. *J Hydrol* 282:104–115
- Jeelani G, Feddema JJ, van der Veen CJ, Stearns L (2012) Role of snow and glacier melt in controlling river hydrology in Liddar watershed (western Himalaya) under current and future climate. *Water Resour Res* 48
- Khadka D, Babel MS, Shrestha S, Tripathi NK (2014) Climate change impact on glacier and snow melt and runoff in Tamakoshi basin in the Hindu Kush Himalayan (HKH) region. *J Hydrol* 511:49–60
- Maksym T, Jeffries MO (2000) A one-dimensional percolation model of flooding and snow ice formation on Antarctic sea ice. *J Geophys Res Oceans* 105:26313–26331
- Mohammed IN, Tarboton DG (2014) Simulated watershed responses to land cover changes using the regional hydro-ecological simulation system. *Hydrol Process* 28:4511–4528
- Molotch NP, Blanken PD, Williams MW, Turnipseed AA, Monson RK, Margulis SA (2007) Estimating sublimation of intercepted and sub-canopy snow using eddy covariance systems. *Hydrol Process* 21:1567–1575
- Pan Y, Birdsey RA, Phillips OL, Jackson RB (2013) The structure, distribution, and biomass of the world's forests. *Annu Rev Ecol Evol Syst* 44:593–622
- Piao S et al (2010) The impacts of climate change on water resources and agriculture in China. *Nature* 467:43–51
- Pomeroy JW, Parviainen J, Hedstrom N, Gray DM (1998) Coupled modelling of forest snow interception and sublimation. *Hydrol Process* 12:2317–2337
- Pomeroy JW, Gray DM, Hedstrom NR, Janowicz JR (2002) Prediction of seasonal snow accumulation in cold climate forests. *Hydrol Process* 16:3543–3558
- Pomeroy JW, Gray DM, Brown T, Hedstrom NR, Quinton WL, Granger RJ, Carey SK (2007) The cold regions hydrological process representation and model: a platform for basing model structure on physical evidence. *Hydrol Process* 21:2650–2667
- Pomeroy J et al (2008) Spatial variability of shortwave irradiance for snowmelt in forests. *J Hydrometeorol* 9:1482–1490
- Pomeroy J, Fang X, Ellis C (2012) Sensitivity of snowmelt hydrology in Marmot Creek, Alberta, to forest cover disturbance. *Hydrol Process* 26:1892–1905
- Reuelto J et al (2015) Canopy influence on snow depth distribution in a pine stand determined from terrestrial laser data. *Water Resour Res* 51:3476–3489
- Robinson DA, Frei A (2000) Seasonal variability of Northern Hemisphere snow extent using visible satellite data. *Prof Geogr* 52:307–315
- Satyawali PK, Singh AK (2008) Dependence of thermal conductivity of snow on microstructure. *J Earth Syst Sci* 117:465–475
- Schweizer J, Jamieson JB, Schneebeli M (2003) Snow avalanche formation. *Rev Geophys* 41
- Schweizer J, Kronholm K, Jamieson JB, Birkeland KW (2008) Review of spatial variability of snowpack properties and its importance for avalanche formation. *Cold Reg Sci Technol* 51:253–272
- Sturm M, Holmgren J, König M, Morris K (1997) The thermal conductivity of seasonal snow. *J Glaciol* 43:26–41
- Sundstrom N, Gustafsson D, Kruglyak A, Lundberg A (2013) Field evaluation of a new method for estimation of liquid water content and snow water equivalent of wet snowpacks with GPR. *Hydrol Res* 44:600–613
- Surazakov AB, Aizen VB, Aizen EM, Nikitin SA (2007) Glacier changes in the Siberian Altai Mountains, Ob river basin, (1952–2006) estimated with high resolution imagery. *Environ Res Lett* 2
- Takala M et al (2011) Estimating northern hemisphere snow water equivalent for climate research through assimilation of spaceborne radiometer data and ground-based measurements. *Remote Sens Environ* 115:3517–3529
- Techel F, Pielmeier C (2011) Point observations of liquid water content in wet snow—investigating methodical, spatial and temporal aspects. *Cryosphere* 5:405–418
- Varhola A, Coops NC, Weiler M, Moore RD (2010) Forest canopy effects on snow accumulation and ablation: an integrative review of empirical results. *J Hydrol* 392:219–233
- Wang Q, Shi J, Chen G, Xue L (2002) Environmental effects induced by human activities in arid Shiyang River basin, Gansu province, northwest China. *Environ Geol* 43:219–227
- Zhong X, Zhang T, Wang K (2014) Snow density climatology across the former USSR. *Cryosphere* 8:785–799
- Zhou J, Kinzelbach W, Cheng GD, Zhang W, He XB, Ye BS (2013) Monitoring and modeling the influence of snow pack and organic soil on a permafrost active layer, Qinghai-Tibetan Plateau of China. *Cold Reg Sci Technol* 90–91:38–52
- Zhou J, Pomeroy JW, Zhang W, Cheng G, Wang G, Chen C (2014) Simulating cold regions hydrological processes using a modular model in the west of China. *J Hydrol* 509:13–24